24th COBEM - 2017

24th ABCM International Congress of Mechanical Engineering
December 3-8, 2017, Curitiba, PR, Brazil

COBEM-2017-2391
DEVELOPMENT AND CHARACTERIZATION OF A 2D PHASED ARRAY ULTRASSONIC TRANSDUCER FOR UNDERWATER APPLICATIONS

Estevão Patricio Rodrigues
Timoteo Francisco de Oliveira
Flávio Buiochi
School of Engineering at the University of São Paulo, Department of Mechatronic Engineering, Laboratory of Ultrasound, São Paulo, São Paulo, Brazil 05508-010.
e-mails: estevaopatricio@usp.br; timolf@hotmail.com; fbuiochi@usp.br

Abstract. *A 2D phased array ultrasonic transducer can electronically deflect and focus acoustic beams in a 3-D space. These characteristics make it attractive for underwater applications such as sonar, to detect and identify reflective interfaces (e.g. objects, ocean floor, and shipwrecks). This paper presents the modeling, construction and characterization processes of a 2D phased array prototype, composed by sixteen 5-mm square elements of Pz37 piezoelectric ceramic with a frequency of 500kHz. A matching layer of alumina/epoxy composite is added to optimize the acoustic transmission. In order to optimize the pulse-echo response, three types of backing layers were tested: air, water, and tungsten/epoxy composite. The acoustic field measured was compared to the theoretical model of a plane piston impulse response, simulated in MATLAB.*

Keywords: *SONAR, 2D phased array, ultrasonic, underwater*

1. INTRODUCTION

An underwater transducer is also known as SONAR (SOund Navigation And Ranging). It usually operates in the pulse-echo mode (Sherman and Butler, 2016), working actively and passively. It is considered active when it emits acoustic signals that will be reflected by an interface between media of different acoustic impedances. It is considered passive when it detects and localizes objects that emitted sounds. Unlike underwater optical cameras, sonar sensors can produce images even in turbid water, with greater range of vision and providing useful 3-D information of objects (Trucco, *et al*., 2008). However, the resolution of the acoustic image is typically lower than that of the optics because the wavelength of the ultrasound is much larger than that of light (Trucco, *et al*., 2008).

A 2D phased array ultrasonic transducer can be used as a sonar to improve the image quality. It is composed of many piezoelectric elements that can be individually controlled to transmit and receive acoustic beams. Each of the elements is a source of ultrasound that can be activated at a different instant of time. When the elements are excited by electric pulses with delays previously defined by delay laws, a front of wave steered and focused at a given point is produced (Schmerr Jr., 2015). Given all these characteristics, a 2D phased array ultrasonic transducer is useful for many underwater applications, such as for 3-D imaging for unmanned undersea vehicles (UUVs) to obstacle avoidance, mines hunting, navigation, and imaging system for orientation of divers in low visibility conditions (Johnson, et al., 2002).

This paper presents the process of modeling, construction and characterization of a 2D phased array ultrasonic transducer prototype for underwater applications. In order to optimize the acoustic emission and to improve the echo response, three types of backing layer material (air, water, and tungsten/epoxy composite) were evaluated and compared. The characterization of the transducer was made by measuring its electrical impedance and its pulse-echo response. Acoustic simulations with real impulse responses were made for all three transducer assemblies to be compared to the acoustic field measured with a needle hydrophone.

2. TRANSDUCER DESIGN

The main constitutive parts of the 2D phased array ultrasonic transducer prototype presented in this paper are the piezoelectric active elements, the matching layer, and the backing layer (Fig. 1). Each one of these components has direct influence in the transducer performance. Active elements are made of lead zirconate titanate (PZT) piezoelectric ceramic, because this ferroelectric material provides mechanical resistance, high electromechanical conversion

efficiency and low intrinsic losses (Bronzino, 2006). On the other hand, piezoelectric ceramics have higher acoustical impedance than that of water and this produces unwanted reflections. To optimize the acoustic transmission a matching layer was added on the frontal face of the transducer. In order to improve the transmission and the bandwidth of the acoustic signals a backing layer is included on the backward face of the transducer. For electric connections thin wires are soldered between element electrodes and the connector (using a micro-coaxial cable). The transducer is held inside high density foam housing. The main components of the 2D phased array transducer prototype are designed below.

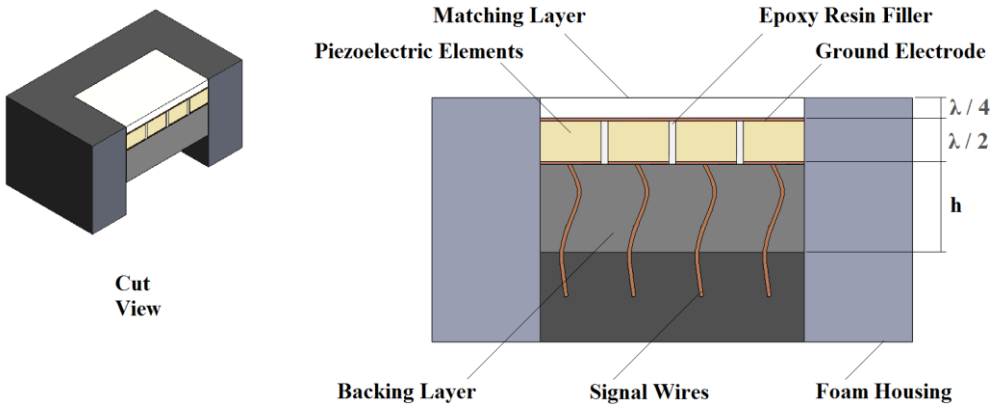

Figure 1. Main parts of the 2-D phased array ultrasonic transducer prototype

2.1 Active Elements Array

A 2-D phased array ultrasonic transducer is composed by piezoelectric ceramic elements arranged as shown in Fig. 2. A piezoceramic performs the conversions of electrical into mechanical energy and vice-versa. Its thickness is half wavelength. The pitch, that is the space of center to center of piezoceramic elements, should be no more than half wavelength to avoid grating lobes (Turnbull and Foster, 1991).

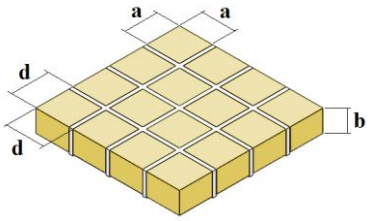

Figure 2. Dimensions of the 2D array elements, where element side is “a”, thickness is “b”, and the pitch is “d”

While this practice is useful for nondestructive evaluation and for medical imaging transducers, where the pulse-echo range is not so critical, for underwater applications larger elements are desired to improve the emission and reception of acoustic energy. Recently, Ehrhardt et al., 2016 presented a real-time high-resolution 3-D sonar camera for deep-water operation, whose pitch is two wavelengths. For decoupling lateral and thickness vibrations a nearly square cross-section should be avoided, such that the ratio of a by b must be less or equal to 0.6 or higher or equal to 10 (Bronzino, 2006).

2.2 Matching and Backing Layers

The addition of matching layer and backing layer are needed to improve the acoustic energy emitted and the bandwidth. The design of both layers is associated with the acoustic impedance of their materials. Materials with equal acoustic impedance do not produce reflections of acoustic waves. However, different acoustic impedances make partial transmission and reflections of the acoustic wave, depending on the transmission and reflection coefficients. The acoustic impedance Z (rayl) is calculated by the product $\rho.c$, where ρ is the fluid density, and c is the wave propagation velocity in the medium that is the product of $\lambda.f$, where λ is the wavelength and f is the frequency. Table 1 provides useful acoustic impedance information to design the matching layer and the backing layer.

The matching layer optimizes acoustic transmission between the array elements and the medium. Its thickness must be a quarter of a wavelength, and the acoustic impedance is the geometric mean of the acoustic impedances of water and of piezoceramic (Cheeke, 2012).

A backing layer lowers the number of cycles of signal emitted by the transducer attenuating the waves emitted backwards. This increases the bandwidth of signal and the axial resolution. But this is obtained at cost of loss of energy that could be emitted, decreasing the operational range (Bronzino, 2006). For optimizing the attenuation of backwards waves the acoustic impedance of ceramic *Zc* and the acoustic impedance of the backing layer *Zb* must be equal.

The attenuation coefficient of a material for a specific frequency, given in dB/cm (ASTM, 2003), can be evaluated by measuring the amplitude of longitudinal waves crossing a sample material immersed in water, as given in Eq. (1) and Eq. (2) (Wu, 1996), where *Ti* is the coefficient of energy transmitted to the sample (indices *1* and *2* are water and sample material, respectively), *Al* and *Ao* are the amplitudes of the signal measured with the sample and without the sample, respectively, and *h* is the sample thickness. After αl is determined, the backing height, *h* (see Fig. 1), is evaluated according to the desired attenuation.

$$\alpha l = \frac{\log(Ti.Al/Ao)}{h} \tag{1}$$

$$Ti = \frac{4.Z1.Z2}{(Z1+Z2)^2} \tag{2}$$

With the transmission coefficients calculated by Eq. (2), presented in the Tab. 1, it is verified that a backing layer with very low acoustic impedance reflects almost all acoustic energy of the backward wave to the emission direction. This improves the acoustic emission but it does not reduce the number of cycles, resulting in a narrow band and long duration pulse. The use of tungsten as the backing layer material attenuates about fifty percent of the backward waves energy, so a narrow pulse is expected.

Table 1. Acoustic properties.

Material	Velocity (m/s)	Density (kg/m^3)	Impedance (MRayls)	*Ti*, for Z1 equal Z_{Pz37}
Air [*]	330	1.2	0.0004	~0
Water [*]	1480	1000	1.48	0.28
Tungsten [**]	5233	18700	98	0.52
Epoxy Resin [**]	2554	1170	3	0.49
Aluminum [**]	6422	2699	17.33	~1
Pz37 [***]	2727	6600	18	1

References: [*] Schmerr and Song, 2007; [**] Sayers and Tait, 1984; [***] Ferroperm Piezoceramics A/S.

2.3 Acoustic Field Modeling

A usual model for describing a 2D phased array ultrasonic transducer is the *piston transducer model* (Fig. 3). This model assumes that each element of *S* area is a *v* normal velocity source acting like a piston (Schmerr Jr., 2015). These "pistons" are embedded on a rigid baffle so that just piston faces can act, i.e., *v*(x, y, z=0, f or t domain) is equal to 0 if out of *S*.

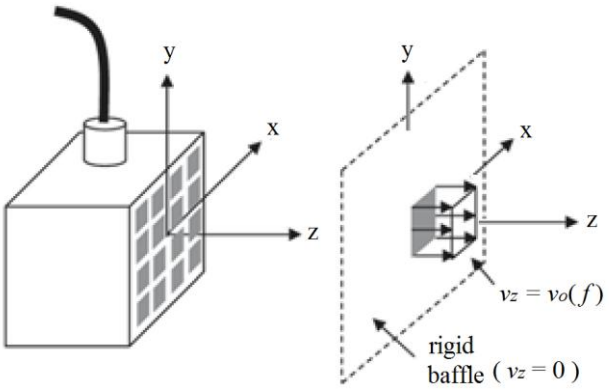

Figure 3. 2D phased array ultrasonic transducer modeled as a plane piston. Each piston is an acoustic source whose face oscillates with a normal velocity function *vo*. (Schmerr Jr., 2015)

The acoustic field is evaluated from the transient pressure function that can be calculated from the velocity potential impulse response function, namely h(R, t). The potential velocity of the piston radiator that area S, excited by a Dirac

velocity pulse $\delta(t)$, observed at a point P distant R from the piston, can be evaluated from the Rayleigh integral given by Eq. (3), where $vn(x,y).\delta(t)$ is a Dirac form normal-component velocity pulse (Piwakowski, B., and Sbai).

$$h(R,t) = \frac{1}{2.\pi}\int_S \frac{vn(x,y).\delta(t-R/c)dS}{R} \tag{3}$$

For pistons with rectangular geometries, such as the elements of the transducer designed in this paper, San Emeterio, and Ullate, 1992, presented a closed-form solution for the velocity potential impulse response (Fig. 4(a) and Fig. 4(b)). Their solution allows computation of pressure fields with realistic excitations directly in the time domain.

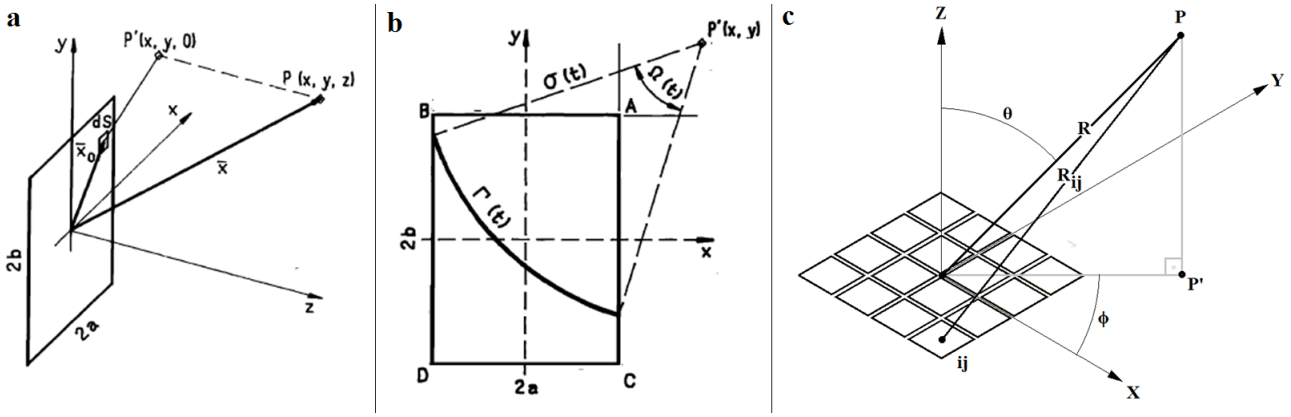

Figure 4. Geometry and coordinate system for the impulse response of a rectangular piston (a) and (b)[*] and for evaluating the delays of a 2D phased array (c) ([*]San Emeterio, and Ullate, 1992)

The integral of Eq. (3) is evaluated, obtaining Eq. (4), where Ω is the angle subtended at P' by the arc intersected by the aperture on a circumference with the center at P', and radius σ(R,t).

$$h(R,t) = \frac{c..\Omega(R,t)}{2.\pi} \tag{4}$$

The transient pressure that is produced by the piston vibration is given by Eq. (5), where ρ is the density of the medium, * is the convolution operation, and *vn* is the normal-component of velocity of piston (San Emeterio, and Ullate, 1992).

$$p(R,t) = \rho\frac{\partial vn(t)}{\partial t} * h(R,t) \tag{5}$$

In order to obtain the acoustic field produced by a 2D array transducer applying delay laws to steer and focus in P, the term of a single element velocity potential impulse response in Eq. (5) is exchanged by the array velocity potential impulse response, that is given by (Turnbull and Foster, 1991) Eq (6), where elements $i,j \in [-N,N]$, and Δt_{ij} is the relative time delay between element ij and the coordinate origin that is given by Eq. (7). To avoid negative time delay, the farthest element to focal point is set to zero delay. Fig. 4(c) shows the geometry and parameters to evaluate the velocity potential impulse response of the array.

$$h_a(R,t) = \sum_{i=-N}^{N}\sum_{j=-N}^{N} h_{ij}(R, t-\Delta t_{ij}) \tag{6}$$

$$\Delta t_{ij} = \frac{R - Rij}{c} \tag{7}$$

3. PROTOTYPE CONSTRUCTION

The piezoelectric ceramic utilized to obtain the active elements of the array is the Pz37, with frequency of 500 kHz and acoustic impedance of 18 MRayl. According to the manufacturer datasheet (Ferroperm Piezoceramics), this ceramic can be applied for underwater and nondestructive testing transducers. This piezoceramic has low acoustic impedance, favoring the acoustic matching with the water, which consequently improves the acoustic emission. The

array elements were fabricated through dicing and filled technique. A precision cutting automatic machine ISOMET 4000 was utilized to make a set of grooves in transversal directions on the Pz37 plate. The sixteen square elements were separated by a 200 um blade such that each element has 5 mm sides, resulting in a pitch of approximately 5.3 mm (Fig. 5(a)). Inter element kerfs were filled with epoxy resin Araldite® GY 279 and hardener Aradur® 951 from Huntsman International LLC. To avoid resin leakage during the filling process, a thin phenolic plate shield held with wax and melted paraffin was attached to the sides of array (Fig. 5(b) and Fig. 5(c)).

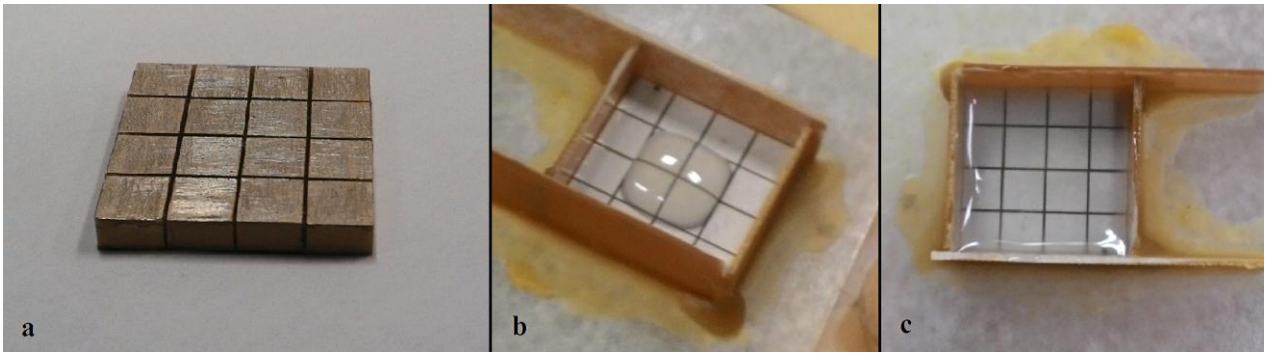

Figure 5. Array obtained from dicing a Pz37 piezoceramic plate (a); Filling process with epoxy resin (b) and (c)

A composite of alumina with the same type epoxy used in the array filling was prepared for matching layer construction. Its acoustic impedance was approximately 5.2 MRayl and was calculated usingthe values of Tab. 1. Oliveira (2015), characterized a sample of matching layer material with twenty five percent of alumina volume resulting in Z, ρ, and c equal to 5.26 MRayl, 1863 kg/m3, and 2823 m/s, respectively. This composite was utilized in the matching layer of the transducer prototype. The matching layer thickness calculated for a 500 kHz frequency is 1.41 mm. Initially, the matching layer construction followed the same process presented in Fig. 5(b) and Fig. 5(c). The plate shield was filled to approximately 1.5 mm, and after the cure of composite, was sanded until 1.41 mm.

The electric interconnections was made with 150-um diameter wires, soldered on the array element electrodes utilizing Sn-Pb alloy solder. A connector made with a pin bar that is much used in electronic boards was soldered to the wires. A foam housing was attached to the transducer to support the connectors, to protect the transducer, and to make the air backing layer.

Three setups of backing layer were tested (Fig. 6), using the same transducer prototype. Before addition of composite backing layer, all measurements were made with water and air backing transducer, respectively. In order to avoid a high attenuation of the acoustic energy and to increase the emission, the chosen acoustic impedance of the composite is half of the acoustic impedance of the Pz37 piezoceramic. Once the backing acoustic impedance was defined, the tungsten and epoxy quantities were calculated based on the model presented by Sayers and Tait, (1984). The graphics generated by this model help to determine the volume ratio of tungsten. For 9 MRayl the volume ratio of tungsten/epoxy composite is 0.3 and the αl calculated from Eq. (1) is 16dB/cm/MHz. The preliminary backing filling was 7 mm of height resulting in around 12 dB of attenuation. The intended 30 dB of attenuation was not accomplished because by the measurements performed, with the first filling, the signal amplitudes presented an important decrease. On the other hand, the addition of some more composite could make the transducer unfeasible for underwater application.

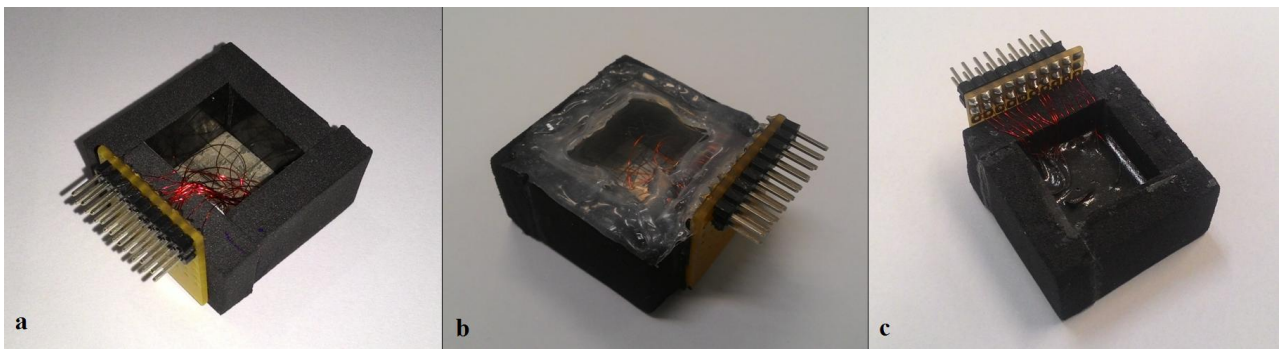

Figure 6. Backing setups: no backing (a); air backing (b); epoxy/tungsten composite backing (c)

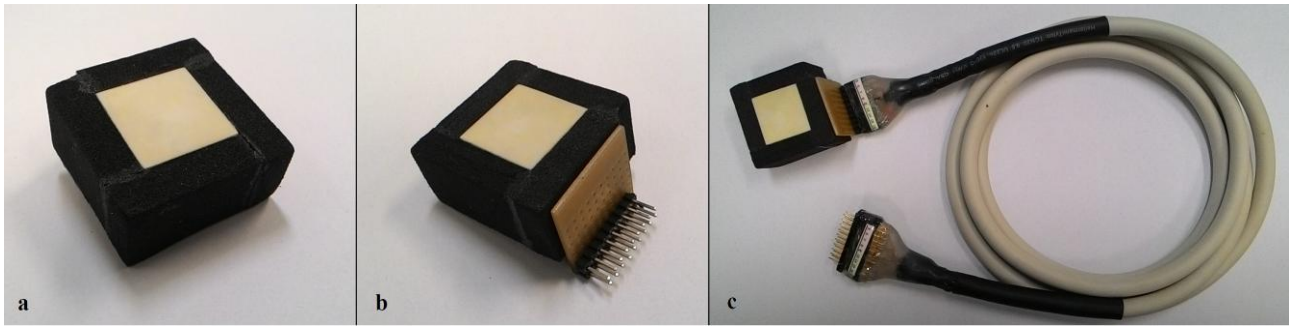

Figure 7. Frontal view (a); Transmit-receive connector (b); Prototype accomplished with interconnection cable (c)

4. PROTOTYPE CHARACTERIZATION AND RESULTS

Fig. 8 shows the electrical impedance measured with an Agilent 4294A impedance analyzer. Each array element was interconnected from its connector pin to the impedance analyzer by a pair of short wires, with transducer in air (no load). For better visualization only the four center elements of the transducer prototype were depicted.

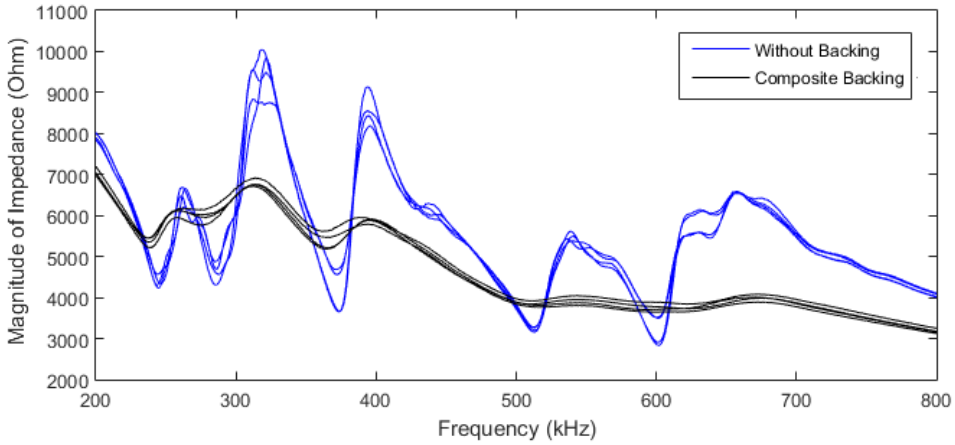

Figure 8. Electrical impedances of four central elements of the array transducer with two backing setups

To evaluate the waveform, the resonance frequency and the bandwidth, the echo was measured (Fig. 9). The transducer prototype was immersed in water and a plane brass reflector was positioned 50 mm apart from the transducer face. The emission and reception of signals were made for each element of the array, with an Olympus Panametrics-NDT 5077PR square wave pulser/receiver, that was configured for all measurements to 100 Hz of pulse repetition frequency, 100 V pulser voltage, 500 kHz transducer frequency, 0 dB gain, high pass frequency disabled, and 10 MHz low pass filter. The data acquisitions were made by an Agilent Infiniium MSO8104A 1 GHz, adjusted for 500 MHz of sample frequency. The sensitivity of each element is shown in Fig. 10, and the summary of the measurements are in Tab. 2. Figure 11 shows the normalized peak-to-peak amplitudes of echoes from all elements, individually, and these values were used in the acoustic field simulations for weighing (apodization) the *vn* amplitudes.

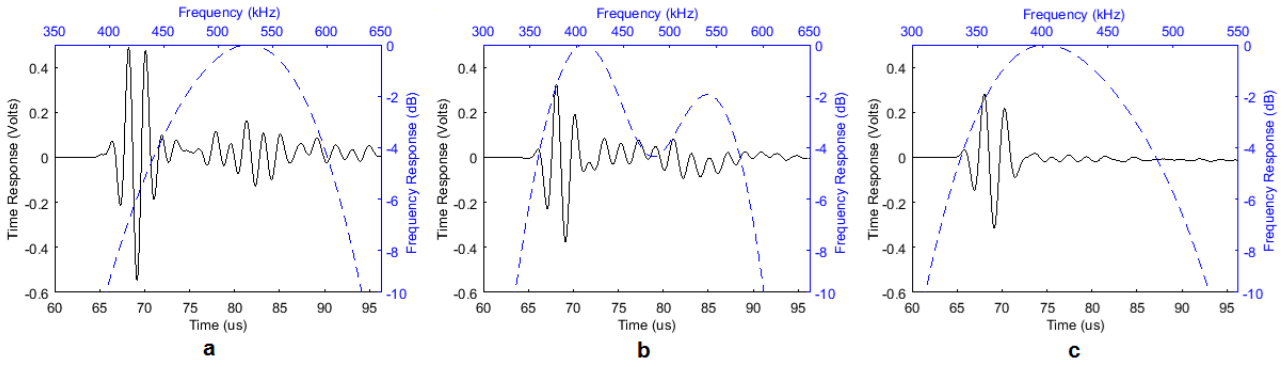

Figure 9. Echo response from element 6 of transducer with air backing (a), water backing (b) and composite backing (c)

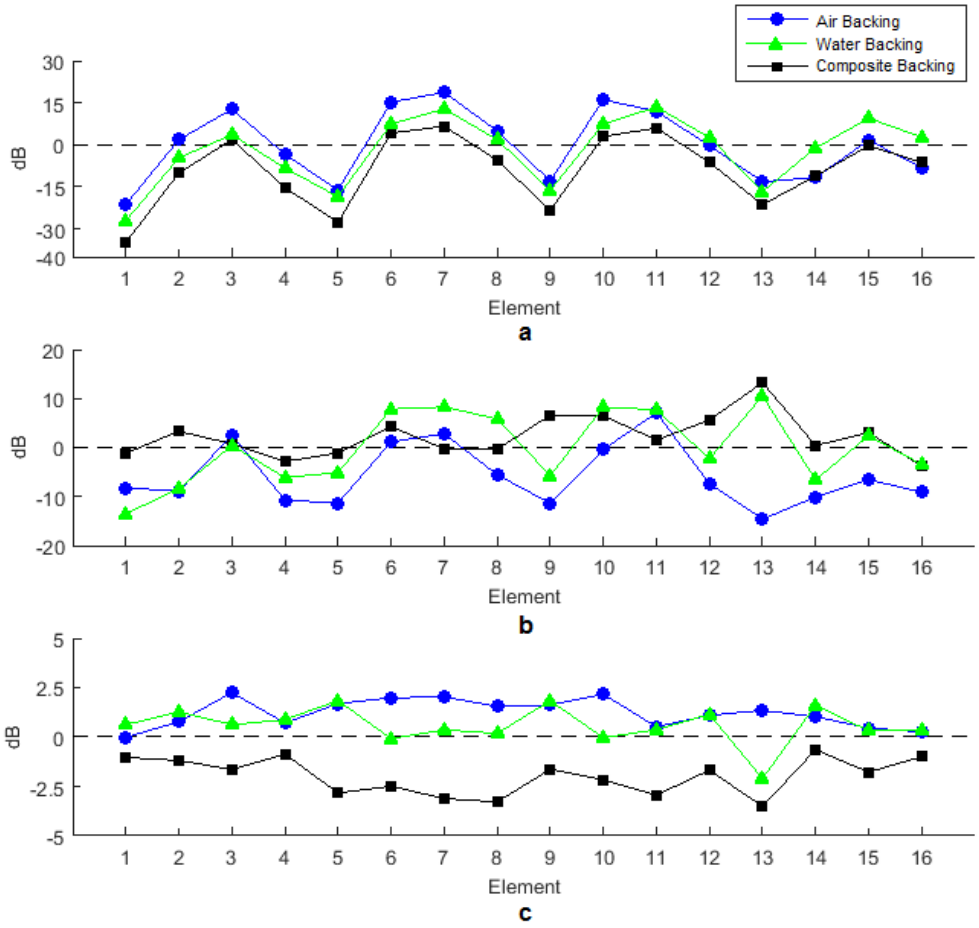

Figure 10. Sensitivity relative to overall mean of the peak-to-peak voltage (a), bandwidth frequency (b), and central frequency (c), measured in pulse-echo mode

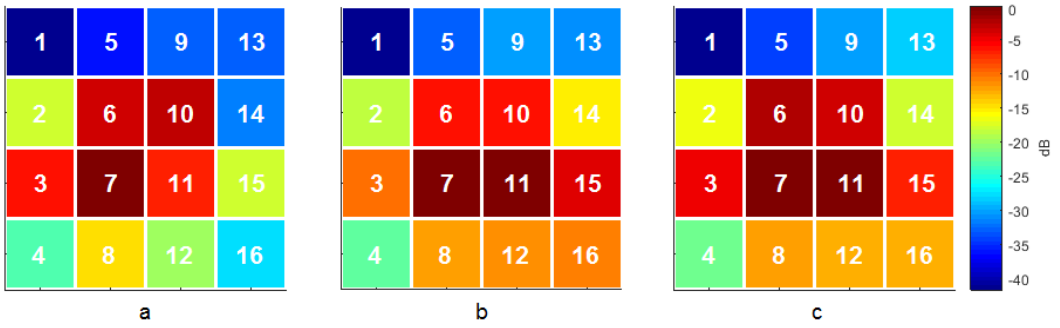

Figure 11. Echo response (peak-to-peak voltages) of transducer with backings made of air (a), water (b), and composite (c)

Table 2. Time and frequency responses of transducer with three backing types

Measurement	Peak-to-Peak (Volts)				Bandwidth -6dB (%)				Central Frequency (kHz)			
Backing Type	Air	Water	Tungs.	Overall	Air	Water	Tungs.	Overall	Air	Water	Tungs.	Overall
Maximum	1.23	0.95	0.67	1.23	48.3	57.3	65.7	65.7	525.7	515.2	455	525.7
Minimum	0.16	0.12	0.08	0.08	16.3	17.2	28	16.3	469.4	423	394	394
Mean	0.57	0.51	0.37	0.48	26.8	36	38.7	33.9	499.5	484	425.8	469.8
Standard Deviation	0.35	0.26	0.19	0.28	9.2	12.9	9.3	11.6	17.9	22.4	19.9	37.7

For simulation of the acoustic field produced by the array transducer, the software inputs used were: density and acoustic speed of the medium of 1000 kg.m^3 and 1500 m/s, respectively; element dimensions of a=5 mm and d=5.3

mm; spatial step of 1 mm; sample rate frequency of 50 MHz, the same of the impulse responses measured (Fig. 12); and the normal velocity of pistons (elements) was given by the impulse response of the element 11, that presents a good sensitivity for all the backing setups used on the transducer prototype.

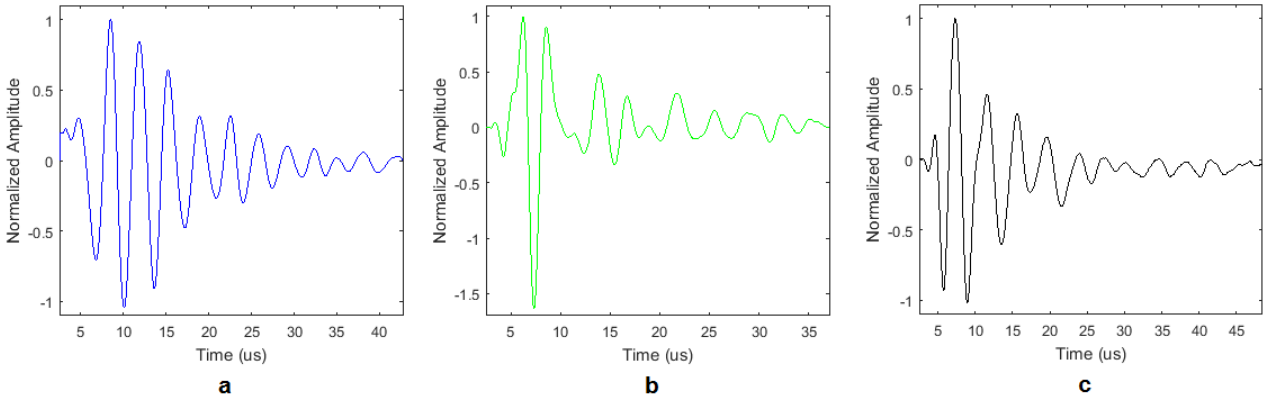

Figure 12. Impulse responses of element 11 of transducer with air backing (a), water backing (b), and composite backing (c). The signals were used for simulations of the acoustic field generated by these transducers.

The acoustic field was initially measured for the transducer without backing, i.e., water backing, using the same transmitter/receiver setup of pulse-echo measurements, except for the sample rate frequency of 50 MHz. All elements were pulsed at the same time, without delay laws. Deflection and focusing measurements were not performed due to hardware limitations of the transmitter / receiver, which would require a multi-channel system for excitation and independent reception by the elements with signal delay laws. The acoustic field was simulated with the impulse response of water backing transducer, depicted in Fig. 12(b). The acoustic field simulated was compared to that measured, presented in Fig. 13. A good agreement between them is observed, mainly after the focal point, where the maximum acoustic pressure occurs, which in this case is around 45 mm. However, before the focal point, known as near field, an irregular aspect is present, because constructive and destructive interferences occur in this region.

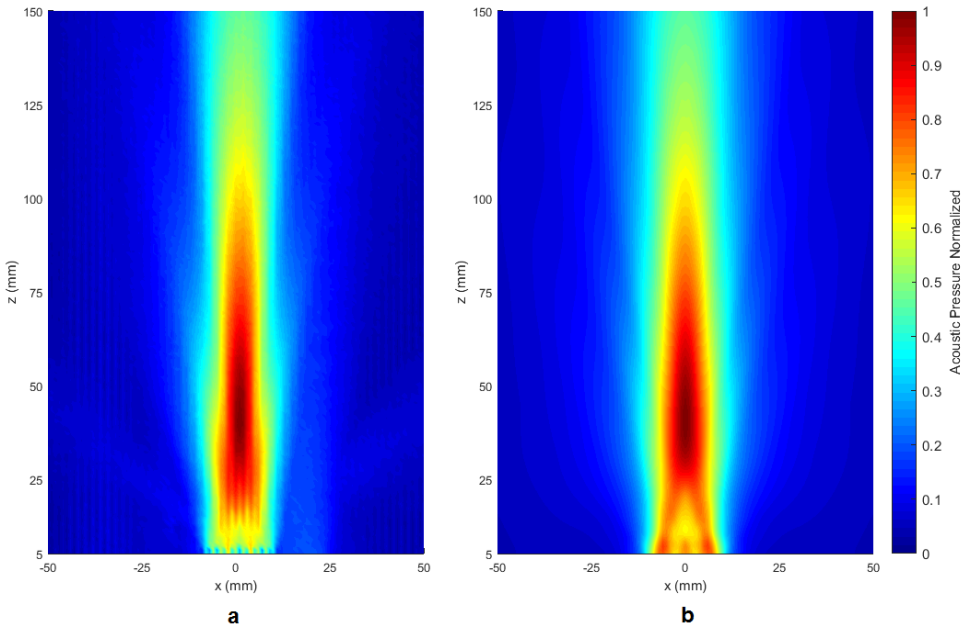

Figure 13. Acoustic field of transducer with water backing, measured (a), and simulated (b), at y=0 mm; natural focus

The transverse acoustic profiles, presented in Fig. 14, allow verifying the main lobe width that determines the transducer resolution. The width of the main lobe is determined at half maximum amplitude (Turnbull and Foster, 1991). To evaluate the algorithm developed for acoustic simulations, seven points in the acoustic field in the transversal direction were measured. The results show that there was a good agreement between the measured values and the simulated curves, since in all cases there is a tendency for the points to meet the curve. There is no perfect symmetry between the simulated graphs. This is due to the effect of the apodization of the vibrations of the elements (Fig. 11) which were also included in the simulation of the transducers, for closer to real results.

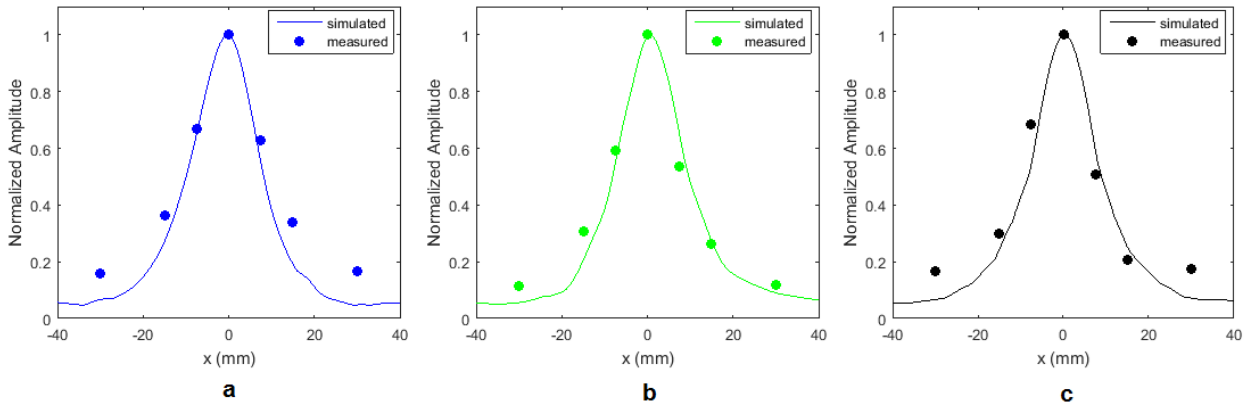

Figure 14. Transverse acoustic profile, measured and simulated, of transducer with backing of air (a), water (b), and composite (c), at z=45 mm; y=0 mm; natural focus (no delay laws)

The ability of the transducer prototype to deflect and to focus the acoustic beam was evaluated in the simulations, using as inputs the values measured during the characterization of the prototype. The simulations of the acoustic field, in a plane parallel to the transducer face (Figure 15), show that it is possible to deflect and focus the acoustic beam in a three-dimensional region. Also, there are grating lobes, which occur when a transducer has a pitch between elements greater than half of a wavelength.

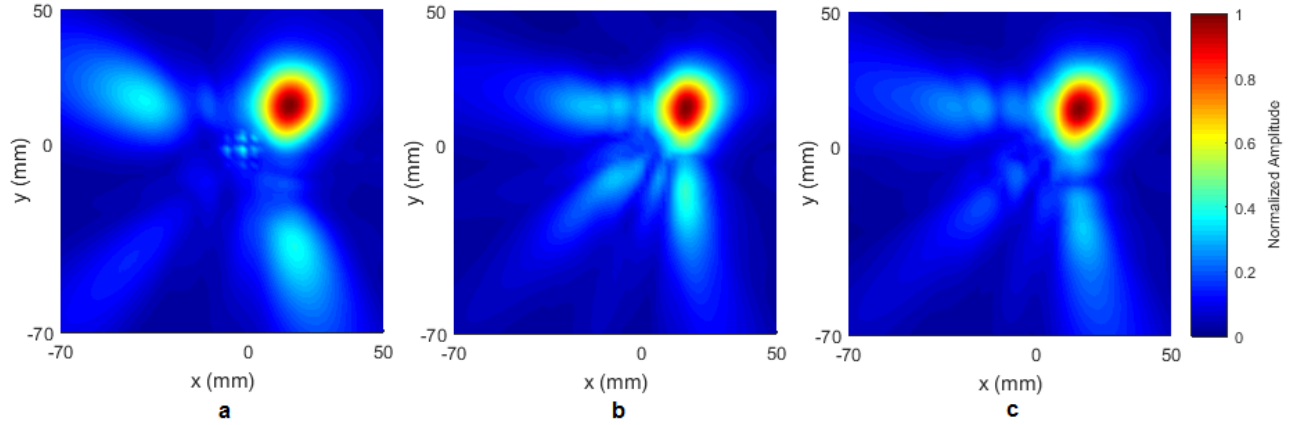

Figure 15. Acoustic field simulations of transducer with backing of air (a), water (b), and composite (c), at z=50 mm, focusing in a 3-D space, at R=1000 mm; θ=25^o; ϕ=45^o

The grating lobes are easily evaluated by the graph of the pressure distribution according to the angle, shown in Fig. 16. The magnitude of the grating lobe increases as the deflection angle increases. Both in the case of focusing and deflection of the beam in a 2D plane (Fig. 16) and in a 3-D region (Fig. 15), for a given angle, the amplitudes of the grating lobes changed according to the type of backing used.

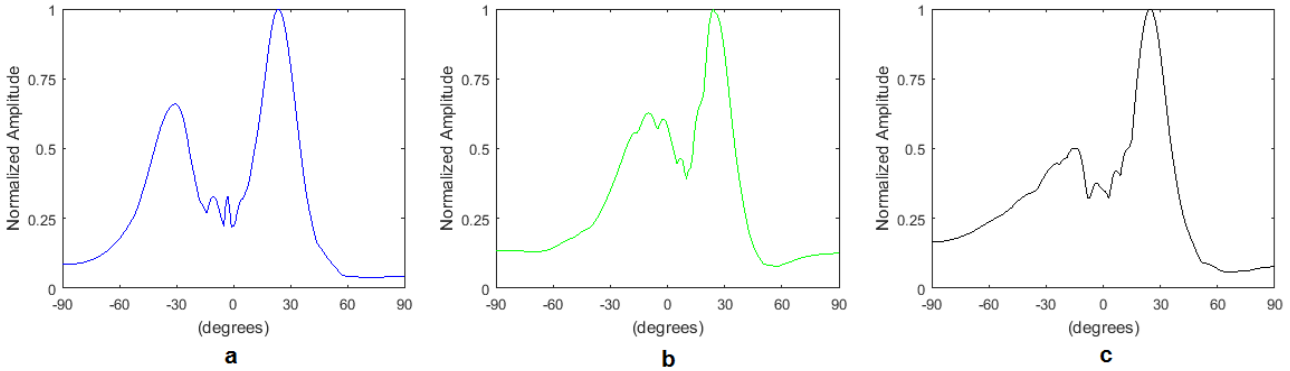

Figure 16. Simulated acoustic field profile of transducer with backing of air (a), water (b), and composite (c), at 45 mm of radius in the plane x z (y=0 mm); 2D focusing at R=1000 mm; θ=25^o; ϕ=0^o

In the case of the air-backed transducer, there was a larger, and more defined spacing between the main lobe and the grating lobe. This beam separation creates artifacts in the image and decreases the amount of energy emitted in the

direction of focus, decreasing the transducer operating range and worsening image contrast. The transducer with water backing presents an approximation of the main and grating lobes, tending to converge the emitted energy towards the region of interest. The composite backing transducer also decreased the amplitude of the grating lobe and brought it further closer to the main lobe, concentrating the energy emitted towards the region of interest. According to these results, the composite backing presents the better performance because it favors the directivity of the main lobe toward the focus, which should increase the contrast and the range of image. Also it has the higher mean of the bandwidth (Fig. 10(b)). However, Fig. 10(a) shows that the pulse-echo sensitivity, for normal incidence, is higher for the transducer with air backing, and intermediate for the transducer with water backing. Therefore, for lower focus deflection, higher amplitude is expected for the air backing transducer, at the cost of a smaller bandwidth in comparison to the water and composite backing transducers. The composite backing improves the regularity of the peak-to-peak echo amplitude in relation to air, and water backing transducers (Fig. 11), decreasing the apodization effect, providing more energy to be transmitted by the transducer. The lower peripheral peak-to-peak amplitude provided by the elements of the transducer may be explained by the housing material, which is soft, and so it does not restrain the movements of lateral modes, causing a loss of energy in the emission.. But the soft housing material can be efficient for acoustic isolation, reducing disturbances induced by the medium.

5. CONCLUSIONS

A two-dimensional phased array transducer prototype was designed, constructed, and characterized. The software developed allowed to simulate and to evaluate three-dimensional deflections and focusing of acoustic beams. The good agreement between simulations and measurements validates the software developed for acoustic field simulations of two-dimensional phased array transducer with square elements. The results are promising for submarine applications because they indicate the feasibility of constructing sonars capable of sweeping a three-dimensional region to detect and reconstruct object images. In the near future, more experiments will be done to measure the acoustic field generated by steering and focusing the beam. A two-dimensional transducer with a 1-3 piezocomposite will also be used for future comparisons.

6. REFERENCES

ASTM E1065-99, 2003. "*Standard Guide for Evaluating Characteristics of Ultrasonic Search Units"*. American Standard of Testing Material (ASTM), 99(5), 1–21. https://doi.org/10.1520/E1065_E1065M

Bronzino, J. D., 2006. "*Biomedical engineering handbook"*, CRC press, United States, third edition.

Cheeke, J. D. N., 2012. "*Fundamentals and Applications of Ultrasonic Waves"*, Second Edition, pp122.

Ehrhardt, M., Becker, F. J., Speicher, D., Fonfara, H., Hewener, H., Fournelle, M., Tretbar, S., 2016. "*Evaluation of a high-resolution real-time capable 3D sonar camera for deep sea operation". OCEANS 2016 MTS/IEEE Monterey, OCE 2016*, *19*, 101–110. https://doi.org/10.1109/OCEANS.2016.7761232

Johnson, J. A., Karaman, M., and Khuri-Yakub, B. T., 2002. "*Phased subarray processing for underwater 3D acoustic imaging"*, Oceans '02 Mts/Ieee, *4*, pp. 2145–2151.

Oliveira, T. F. D. E., 2015. "*Transdutores de ultrassom multielementos lineares flexíveis com sensor de curvatura para superfícies curvas*". Doctoral thesis, University of São Paulo, São Paulo, Brazil.

Piwakowski, B., and Sbai, K., 1999. "*A new approach to calculate the field radiated from arbitrarily structured transducer arrays"*. IEEE transactions on ultrasonics, ferroelectrics, and frequency control, 46(2), 422-440.

San Emeterio, J. L., and Ullate, L. G., 1992. "*Diffraction impulse response of rectangular transducers", 92*(August), 651–662.

Sayers, C. M., & Tait, C. E., 1984. "*Ultrasonic properties of transducer backings*". Ultrasonics, 22(2), 57–60. https://doi.org/10.1016/0041-624X(84)90022-2

Schmerr Jr, L. W., 2015. "*Fundamentals of Ultrasonic Phased Arrays"*, Springer, Switzerland, vol. 215, pp. 3.

Sherman, C. H. and Butler, J. L., 2016. "*Transducers and arrays for underwater sound"*, Springer, Switzerland, second edition, pp. 1

Schmerr, L., and Song, S.-J., 2007. "*Ultrasonic Nondestructive Evaluation Systems: Models and Measurements"*, Springer Science+Business Media.

Trucco A., Palmese M., and Repetto, S., 2008. "*Devising an affordable sonar system for underwater 3-D vision"*, IEEE Trans. Instrum. Meas., vol. 57, no. 10, pp. 2348–2354.

Turnbull, D. H. and Foster, F. S., 1991. "*Beam Steering with Pulsed Two-Dimensional Transducer Arrays"*, IEEE Trans. Ultrason. Ferroelectr. Freq. Control, vol. 38, no. 4, pp. 320–333.

Wu, J., 1996. "*Determination of velocity and attenuation of shear waves using ultrasonic spectroscopy"*. Journal of the Acoustical Society of America, 99(5), 2871–2875.

Ferroperm Piezoceramics A/S. 1 Sept. 2017 <http://www.ferroperm-piezo.com/>.

7. RESPONSIBILITY NOTICE

The authors are the only responsible for the printed material included in this paper.